This is a repository copy of *Dynamic monitoring of glycine crystallisation with low power ultrasound reflection spectroscopy*.

White Rose Research Online URL for this paper:
https://eprints.whiterose.ac.uk/179119/

Version: Accepted Version

Dynamic monitoring of glycine crystallisation with low power ultrasound reflection spectroscopy

Liam Morris[a], Elena Simone[a], Zachary J. Glover[a], Hugh Powell[b], Stéphanie Marty-Terrade[b], Mathew Francis[a], Megan J Povey[a]

[a]School of Food Science & Nutrition, University of Leeds, Leeds, West Yorkshire, LS2 9JT, United Kingdom.

[b]Nestlé Product Technology Centre Confectionery, Haxby Road, York, YO91 1XY, United Kingdom.

Author emails:

Liam Morris: fs13lm@leeds.ac.uk

Elena Simone: e.simone@leeds.ac.uk

Zachary Glover: zachary.glover@arlafoods.com

Hugh Powell: hugh.powell@rdyo.nestle.com

Stéphanie Marty Terrade: stephanie.marty-terrade@rdyo.nestle.com

Mathew Francis: m.francis1@leeds.ac.uk

Megan Povey: m.j.w.povey@food.leeds.ac.uk

Corresponding author: Liam Morris, fs13lm@leeds.ac.uk, School of Food Science & Nutrition, University of Leeds, Leeds, West Yorkshire, LS2 9JT, United Kingdom.

Abstract:

Crystallisation processes are ubiquitous in the food and pharmaceutical industries and the development of process analytical technologies (PAT) for on-line, in situ monitoring is essential to ensure process efficiency and to optimise product quality. Current PAT, many of which are based on electromagnetic waves, have a range of limitations including an inability to accurately measure opaque solutions. Low power (<10 W m^{-2}) pulsed acoustic techniques, such as ultrasound reflectance and velocimetry, have the benefit of being non-material altering, affordable, non-invasive and can study opaque systems without any dilution. Here we present an improved in-situ ultrasound technique which is corroborated with optical turbidity in the measurement of the MSZW of glycine in water with good agreement. A Mann-Whitney U test was conducted, and no significant difference was found in the measurement of the MSZW between the two techniques. Density data were used with velocity measurements from the improved technique to calculate adiabatic compressibility of glycine solutions, which is an important and useful physical property when studying phase transitions. A frequency space analysis has been performed on the acoustic time domain measurements, and the data suggest the presence of scattering bodies in the metastable zone.

Highlights:

- A improved ultrasound technique is shown to accurately monitor crystallisation.
- The optical cloud point can be determined using ultrasound with high accuracy.
- Results agree closely with standard optical turbidity.
- The ultrasound technique may be detecting scattering bodies in the metastable zone.
- The technique may give more information than optical techniques and be used to study structures.

Keywords: Ultrasound, acoustic spectroscopy, crystallisation, acoustics, MSZW, in-situ monitoring

Abbreviations:

URS	Ultrasound Reflection Spectroscopy
MSZW	Metastable Zone Width
FFT	Fast Fourier Transform

1 Introduction:

Crystallisation from solution is an important purification and separation technique. It allows the separation of a solute from a solution to obtain a high purity product. Because of this, crystallisation processes are ubiquitous in many industries. High purity crystals are important for different industries, including the pharmaceutical, chemical and food sectors. Crystals, in addition to being a valuable product in their own right, also impart important qualities when included in a larger matrix including imparting texture in foods, hardness and brittleness in metals and determining solubility and bioavailability in pharmaceutical products. Other crystal properties, such as size and shape distribution and polymorphism can also dramatically affect the quality of a particulate product.

The control of crystal nucleation and growth is paramount to the quality and purity of the product. The saturation point is the temperature at which the solvent is unable to dissolve any more solute at a given solute concentration. At temperatures above the saturation point, the solution is undersaturated and nucleation and crystal growth cannot occur. By reducing the temperature, increasing the concentration or through the addition of an antisolvent, supersaturation, the driving force for crystal nucleation and growth, is generated. A supersaturated solution is either in the metastable zone or in the labile region. In the metastable zone the system is supersaturated, but not of high enough concentration to induce spontaneous primary nucleation of crystals. At

low supersaturation it is possible for crystallisation to occur through the addition of crystals to the solution, known as seeding or secondary nucleation.

The cloud point is the temperature at which stable nuclei are first detected as the supersaturation is generated. The cloud point is an important parameter for determining nucleation kinetics. It is usually combined with solubility data to determine the metastable zone width (MSZW) of a material in specific crystallisation conditions. The MSZW is an important and unique characteristic of each crystal system. The MSZW depends not only on the system (solute/solvent combination and solution purity), but also on the method of supersaturation, the rate at which it occurs and on the hydrodynamics conditions (e.g., stirring rate). Borji and Jourani (2018) define the MSZW (ΔT_{max}) as;

$$\Delta T_{max} = T_0 - T_c \tag{1}$$

Where T_0 is the saturation temperature and T_c the cloud point.

Knowing the width of the metastable zone is vital for the design of industrial crystallisation processes. The MSZW describes how easily a system nucleates in different solvents and at specific temperatures. This information is essential to control the size and shape distribution as well as the crystal purity during crystallisation. In fact, most industrial crystallisation processes are seeded and are operated within the MSZW to promote controlled crystal growth and secondary nucleation over uncontrolled primary nucleation. A good understanding of the MSZW therefore allows for crystal size distribution, habit and purity to be more easily optimised (Ulrich and Strege, 2002).

Process analytical techniques (PAT) are techniques which can be used for optimising manufacturing processes, through the ability to analyse, design or control these processes (Simon et al., 2015). Many techniques, predominantly using electromagnetic wavelengths (e.g., ultraviolet/visible or infrared spectroscopy), are currently used for monitoring crystallisation processes and estimate nucleation kinetics. Techniques commonly used to determine the cloud point include particle counters such as Focused Beam Reflectance Measurement (FBRM) (Burbidge et al., 1995; Fujiwara et al., 2002; Barrett and Glennon, 2002), Fourier Transform Infrared Spectroscopy (FTIRS) (Fujiwara et al., 2002) and optical turbidity (Marciniak, 2002; Parsons et al., 2003; Hennessy et al., 2004; Liang et al., 2004; Correia et al., 2006; Callahan and Ni, 2012). Some less common techniques include densitometry (Marciniak, 2002) and electrical conductivity (Lyczko et al., 2002). Some studies utilised the naked eye as a technique (Sangwal et al., 2014; Rahman and Rahman, 2015), however, this technique is not suitable for work which requires high accuracy and repeatability.

Optical and spectroscopic techniques are limited in the size of crystals they can detect due to wavelength limitations, as well as being sensitive to opaque systems (Povey, 1997; Povey, 2013). Low powered acoustic techniques have the advantage of being non-destructive, economical and being able to measure smaller particle sizes than

most optical methods (Povey, 1997). The use of ultrasound in manufacturing is mostly associated with high power acoustics, and the use of transient cavitation to induce crystal nucleation and growth (sonocrystallisation). High powered ultrasound from a sonotrode (a resonator that produces standing waves) directed into a crystallising solution provides benefits such as control of polymorphic form, higher purity crystals and faster crystallisation (Nalesso et al., 2019). However, sonocrystallisation is a material altering technique, often unsuitable for food grade applications due to contamination and off-flavours caused by degradation of the sonotrode surface which leads to contamination (Povey, 1997; Povey, 2013; Povey, 2016). The associated cavitation also causes oxidative rancidity in fat containing systems. Low power, non-cavitational ultrasound as a non-material altering technique is non-destructive, non-invasive and can study opaque materials without the need for dilution (Awad et al., 2012; Blitz and Simpson, 1995).

Though the use of acoustic techniques as PAT during crystallisation is not widespread, there are some studies which have utilised them in the determination of the MSZW of various materials, both aqueous and non-aqueous: fluoranthene in trichloroethylene (Marciniak, 2002), magnesium sulphate heptahydrate (Al-Jibbouri et al., 2002), borax decahydrate (Gurbuz and Ozdemir, 2003), potassium nitrate (Titiz-Sargut and Ulrich, 2003), coconut oil (Chaleepa et al., 2010) and potassium sulphate (Ulrich et al., 2018). The parameters measured by these acoustic techniques are the ultrasound velocity (speed of a sound wave through the material) and ultrasound attenuation (how much energy is lost and/or scattered over the propagation path in the sample), both of which are dependent on the physical properties of the material. Velocity measurements, when combined with density measurements, allow for the adiabatic compressibility to be measured. The adiabatic compressibility is useful for the determination of the onset of nucleation and crystallisation since the presence of solids appearing within the solution has an overall effect of reducing the compressibility of the solution. Ultrasonic attenuation measurements observe the change in amplitude and are frequency dependent.

At the cloud point, there is typically a large change in both the ultrasound velocity and ultrasound attenuation associated with the appearance of a solid phase dispersed within the solution which has different physical properties to that of the suspending solution. During crystallisation, the solution concentration changes, giving rise to further modification of the ultrasound velocity and attenuation. The change in velocity is due to changes in thermoacoustic properties such as thermal diffusivity, bulk density and adiabatic compressibility during phase transitions in crystallising systems (Akulichev and Bulanov, 1983). These previous studies have lacked a rigorous signal and data processing methodology, which is what we expand on in this study. Furthermore, non-specialised instrumentation was used in these studies, which obscured the full benefit of acoustic techniques being used as PAT.

Ultrasound Reflection Spectroscopy (URS) (Tong and Povey, 2002) consists of a transducer in a pulse echo setup (Figure 1Figure 1). For a detailed account of the

pulse echo setup and its inner workings see García-Álvarez et al., (2013). Multiple authors have demonstrated the effectiveness of URS techniques for monitoring crystallisation processes, although a demonstration of their use as in situ PAT is limited and has not been optimised (Dickinson et al., 1993; Kulmyrzaev et al., 2000; Hindle et al., 2002; Povey et al., 2006; Povey, 2014). The URS system developed for this study, the improved URS, involves the use of an immersion pulse echo transducer constructed as a probe. By using a special probe design, the improved URS can be used in situ and at both laboratory and plant scale (Francis et al., 2019).

Glycine has been selected in this study as a model crystal system to demonstrate the efficacy of the URS. Glycine is the simplest of the amino acids in structure and has three known polymorphic forms, α, β, and γ. The polymorphic form nucleated can be controlled by altering the pH of the solution. In the range of pH 4-9 the α polymorph nucleates and grows while at pH <4 and >9 the γ polymorph is favoured. The solubility of both α and γ glycine are well known (Yang et al., 2008).

In this study, the performance of the improved URS technique is compared with standard optical turbidity to determine the suitability of the technique for the study of aqueous glycine crystallisation including measuring the cloud point and the metastable zone width. Signal processing using Fast Fourier Transform (FFT) and spectral analysis has been used here to demonstrate the wider array of information that can be captured using acoustic methods compared with standard optical methods. Here, concentrated aqueous solutions of glycine are studied. A recent paper quotes sound velocity and density data for dilute solutions (0.05 to 0.38 mol kg^{-1}) of glycine (Sharma et al., 2020) which are not strictly comparable with our data.

2 Materials and Methods:

2.1 Samples and sample preparation:

250 mL samples of >99% purity α-glycine (Fluorochem Ltd, Glossop UK) solutions were prepared at a range of concentrations: 3.71 mol kg^{-1}, 3.51 mol kg^{-1}, 3.31 mol kg^{-1}, 3.11 mol kg^{-1}, 2.93 mol kg^{-1}. The solutions were prepared in a jacketed beaker using a magnetic stirrer at 200 rpm and were heated to a minimum of 5 °C above their saturation temperature for 30 minutes. Solutions were covered with plastic film to minimise evaporation and to keep the solution concentration constant. The pH of each clear solution was measured using a Model HI 208 pH meter (Hanna Instruments, Rhode Island, USA) before starting the cooling profile.

The solubility of the polymorphs of glycine in water is described by Yang et al., (2008). To determine the solubility of the α polymorph, a quadratic was fitted to the published data and is expressed through

$$S = 0.0003T^2 + 0.0482T + 1.6043 \tag{2}$$

Where S is the solubility of glycine in water (mol kg^{-1}) and T is the temperature (°C).

2.2 Improved URS

The improved URS has a 0.25 ” diameter 50 MHz U8411023 broadband transducer (Olympus Panametrics, Waltham, MA, U.S.A) with an adhered quartz buffer rod housed in a SAE 304 stainless steel casing. The device is equipped with a reflector plate at a changeable distance from the buffer rod to allow the path length to be altered for different materials. The measurement principle is described in (Tong and Povey, 2002).
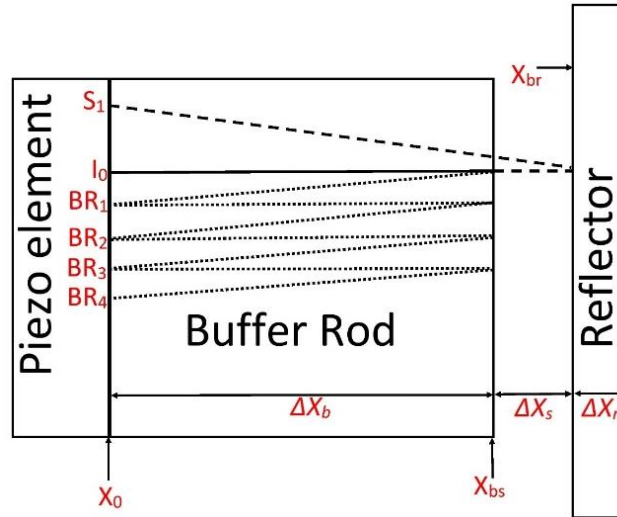
Figure 1 Improved URS measurement principle: Subscript $_b$ represents the buffer rod, $_s$ the sample and $_r$ the reflector. ΔX_b, ΔX_s and ΔX_r represent the lengths of the buffer rod, sample, and reflector, respectively. X_0, X_{bs} and X_{br} are positions in space representing a change in impedance. I_0, BR_1, BR_2, BR_3, BR_4 and S_1 all represent pulses, which are also presented in figure 3. Angled lines representing reverberations are for explication only.

In Figure 1~~Figure 1~~, an ultrasound pulse of intensity I_0 is produced at X_0 by the transducer. The UTEX transmits a 100 V, 2 ns pulse to the transducer which generates a broadband ultrasonic pulse. The pulse travels a distance of ΔX_b and it meets the sample at X_{bs} in time Δt_b. X_{bs} is the position of the sample to buffer rod interface. At X_{bs} some of the sound is reflected and some is transmitted. The reflected signal travels through the buffer rod a distance of ΔX_b in time Δt_b. Upon arrival at X_0, a pulse amplitude of BR_1 is detected of time $2\Delta t_b$. The pulse then continues to reverberate in the buffer rod and reflect at the interfaces, producing further intensities BR_2, BR_3 and BR_4. Further reverberations are present but not shown in Figure 1~~Figure 1~~. Concurrently with the buffer rod reverberations, the transmitted travels through the sample a the distance of ΔX_s until it meets the reflector at X_{br} at time $\Delta t_b + \Delta t_s$. The design of the reflector is such that the impedance is highly mismatched, and as such $R \approx 1$. The pulse travels the distance of ΔX_s until it meets X_{bs} where some signal is transmitted into the buffer rod whilst some is reflected (not shown in Figure 1~~Figure 1~~). The first reverberation in the sample then crosses X_{bs} into the buffer rod and travels a further ΔX_b until it meets X_0 at time $2\Delta t_b + 2\Delta t_s$. Equations (3~~3~~ and (4~~4~~ show how these two measurements are used to determine the time of flight C in the sample.

$$C = \frac{\Delta x_b + \Delta x_s}{\Delta t_b + \Delta t_s} - \frac{\Delta x_b}{\Delta t_b} \tag{3}$$

$$= \frac{\Delta x_s}{\Delta t_s} \tag{4}$$

Figure 2~~Figure 2~~ illustrates the waveforms which are measured by the oscilloscope. To quantify the time of flight, waveforms were exported from the oscilloscope to

MATLAB for post processing. A threshold technique was used to find the first point in the pulse which is <-0.01 volts, every point below this threshold value is recorded. The value corresponding to the start of the sample pulse is taken as the time of flight value, Δt_s, in equation 5.
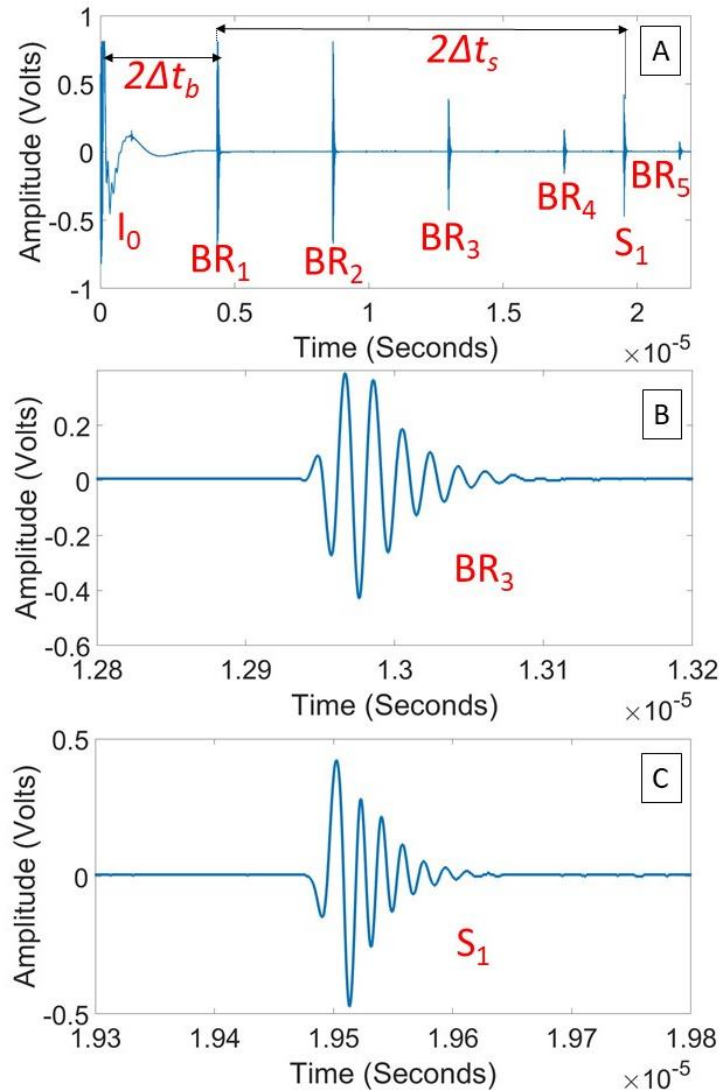

Figure 2 Oscilloscope traces in water: 'BR' represents a buffer rod echo, 'S' represents a sample echo – A is the waveform of several echoes, B is the third buffer rod echo and C is the first sample echo.

To generate the acoustic signal in the URS setup a UTEX UT320 pulser/receiver (UTEX Scientific Instruments Inc., Ontario, Canada) was used. The pulser receiver generated a 100V pulse of 2ns duration with a 200 Hz repetition. A HDO4034 digital oscilloscope (Teledyne Lecroy, New York, USA) connected to the pulser/receiver was set up such that the buffer rod and sample echoes were visible on the trace (Figure 2Figure 2), with adequate windowing to allow for changes in the time of flight with temperature. Waveforms were saved as matrices in MATLAB 2020a (Mathworks,

Massachusetts, United States) and plotted as cartesian co-ordinates. The temperature of the sample was controlled through a jacketed vessel through which M40.165.10 silicone oil (Huber, Kältemaschinenbau AG, Offenburg, Germany) was circulated by a Huber Pilot One Ministat 125 thermostat (Huber, Kältemaschinenbau AG, Offenburg, Germany). The temperature of the sample was monitored with a PT100 thermal probe (Omega Engineering, Manchester, U.K) connected to the thermostat. The sample temperature was fed back to the thermostat allowing accurate and precise temperature control (+/- 0.1 ºC accuracy, +/- 0.01 ºC precision). A mix control eco 1 magnetic stirring plate (2mag, Munich, Germany) was placed under the jacketed beaker with a magnetic flea to stir samples (200 rpm) and maintain homogeneity. In solution, the turbidity and URS probes were placed as close together as possible, and all solutions were continuously stirred to ensure homogeneity. MATLAB 2020a was used to export and process data in real time. Figure 1 shows a schematic of the complete URS setup.
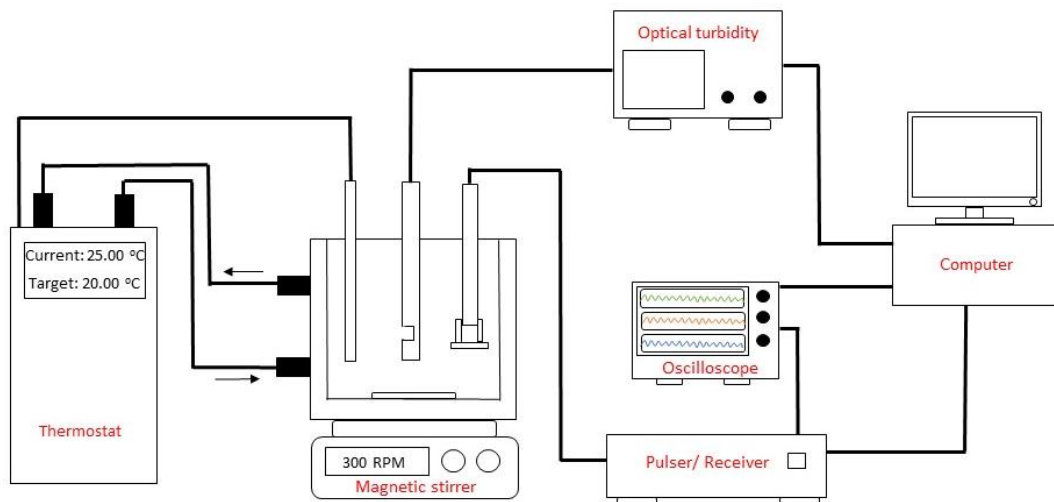

Figure 3 : **URS schematic consisting of the probe, optical turbidity, pulser/receiver, Oscilloscope, PC, thermostat filled with silicone oil connected to a jacketed beaker, and a thermal probe.**

2.3 Time of flight measurement:

MATLAB 2020a was used to export waveforms of the sample pulse every 10 seconds with temperature and time stamps from the oscilloscope. Waveforms were plotted and the time of flight was determined using the "find" function, using a threshold value of - 0.05 V.

2.4 Calibration of sample path length:

The sample path length of the URS changes with temperature due to thermal expansion of the quartz buffer rod. To achieve a high measurement accuracy, it was essential that this is considered. To measure the set path length, a calibration in water

was performed. Water was placed in the jacketed vessel and heated to 50 °C. The URS probe was submerged and left to thermally equilibrate for 1 hour. The water was cooled at -0.1 °C min^{-1} and the waveforms were collected every 60 seconds and exported to MATLAB 2020a. Equation 3 was rearranged to calculate the distance parameter, X which is the sample path length. Time of flight was calculated using the method described in 2.3. Time of flight was used as the time parameter, t in equation 3. The speed sound of water from literature (Chávez et al., 1985; Bilaniuk and Wong, 1993) was used as the speed of sound parameter, C in equation 3. The pathlength was plotted as a function of temperature and a quintic function was fitted to the data. The use of water as a calibrant and the ultrasound velocity data of water from literature (Chávez et al., 1985; Bilaniuk and Wong, 1993) provides a highly accurate ultrasonic velocity measurement. The fitted data produces an accurate equation for the path length at each temperature. The buffer rod to reflector distance was adjustable to account for a wide range of sample attenuation values but was kept fixed in any one experiment. The determined path length agrees with that measured with digital vernier callipers to within measurement error, however, the speed of sound in water calibration method gives a far more accurate determination of the sample distance ΔX_s and hence a much more accurate determination of the speed of sound. Measurement errors are quoted in later sections of this paper.

2.5 Amplitude and attenuation measurements:

The peak to peak amplitude of pulses was measured using the "peak2peak" function in MATLAB 2020a once the waveforms were plotted (amplitude as a function of time). Ultrasound attenuation is then calculated with equation 2 once the initial and live amplitude are recorded.

$$\propto = 20 \cdot log_{10} \frac{A_0}{A}$$

(5)

Where A_0 is the initial amplitude and A is the live amplitude.

2.6 Velocity and adiabatic compressibility measurements:

Ultrasound velocity is calculated through measurement of the time of flight of the sound pulse which has travelled through the sample and then reflected back to the transducer. The time of flight is measured as the delay between the sample pulse and the initial excitation pulse once the waveform has been plotted using MATLAB 2020a. The speed of sound C is given by equation 3.

$$C = \frac{X}{t}$$
(6)

Where X is the path length (twice the distance between the buffer rod sample interface and the sample reflector interface) calibrated using the known speed of sound in water and t is the experimental time of flight. Once the density and velocity is known, the adiabatic compressibility can be calculated using the Wood equation (equation 3).

$$C = \frac{1}{\sqrt{K\rho}} \tag{7}$$

Where C is the speed of sound, K is the adiabatic compressibility and ρ is the density.

Ultrasound velocity and adiabatic compressibility was calculated in real time as a function of temperature using MATLAB 2020a. A quadratic function was fitted to the data and the 95% calculated. 95% confidence intervals were also plotted on their respective figures.

2.7 Optical turbidity:

All transmission data were measured by an Optek Control 4000 optical turbidity probe (Optek-Danulat GmBH, Essen Germany) fitted with a model ASD12-N near IR sensor (wavelength around 700nm). Date were collected every 10 seconds. At the start of each experiment when the solution was undersaturated, the transmission was set to 100%. The data was exported to MATLAB 2020a for further data analysis. Optical transmission data can be visualised and compared as a function of time against improved URS data.

2.8 Glycine crystallisation protocols:

For all crystallisation experiments, glycine solutions were cooled at -0.5 ºC min^{-1} and held at a final temperature of 5 ºC for 15 minutes. Solutions were then reheated at 2 ºC min^{-1} to re-dissolve crystals and held at 5 ºC above the saturation temperature for 30 minutes. To ensure full redissolution had occurred, solutions were visually inspected, and optical transmission measured. This cycle was then repeated at least four times per solution to check repeatability. URS and optical turbidity measurements were collected every 10 seconds and exported to MATLAB 2020a with a live temperature and time stamp.

2.9 Determination of cloud point and MSZW:

MATLAB 2020a was used to determine the point at which a suspected phase change (nucleation or dissolution) occurred in both URS and optical turbidity data. The "findchangepts" function in MATLAB 2020a was applied on the attenuation data from improved URS, and optical transmission data from optical turbidity to determine the temperature at which phase changes occurred. Optical transmission was used as a reference to determine the occurrence of any phase change.

To corroborate the measurements of the two probes, standard deviations were calculated in Excel 2010 (Microsoft, Washington USA). A Mann Whitney U test was performed (n=46), confidence interval 95% using SPSS version 26 (IBM, New York, USA) to determine the difference in optical cloud point measurement temperature between the improved URS and optical turbidity.

To measure the MSZW, cloud point data were averaged and used in equation 1.

2.10 Densitometry:

A DMA 4500 densitometer (Anton Paar, GmBH, Graz, Austria) was used to measure the density of glycine solutions. Before sample analysis, the accuracy of the device was checked against known values for the density of water and the margin of error was on average +/- 3.7×10^{-3} kg m^{-3}, within the instrument error. The glycine solutions were injected into the sample holder and the temperature was raised to 10 °C above the saturation temperature and allowed to equilibrate for 10 minutes. An internal camera was used to ensure the sample chamber was free of bubbles or solid particles. Sample entry and exit points were covered with laboratory plastic film to minimise evaporation. Data points were collected at frequent interval temperatures until 20 °C of supercooling was achieved. At each measured temperature, the sample was allowed to equilibrate for 5 minutes. These density measurements were repeated in quadruplicate and averaged. Standard deviations for population were calculated in Excel 2010 (Microsoft, Redmond Washington).

2.11 Frequency analysis with improved URS:

Relative power spectrum measurement was performed by first using the oscilloscope to FFT the pulse. A memory function recorded a reference frame of the FFT from the starting point of the experiment. The live FFT was subtracted from this reference trace. The sample pulses and spectra were collected and exported to MATLAB 2020a every 10 seconds with the relevant time and temperature. Power spectra were plotted as a function of frequency. Intensities of different frequencies (10 MHz – 50 MHz) were also plotted in 10 MHz intervals as a function of time and plotted with optical transmission as a function of time. These acoustic data were smoothed using robust quadratic regression in MATLAB 2020a.

3 Results and Discussion:

3.1 Determination of pH of glycine solutions:

The pH was between 5.64 and 6.26 at the highest and lowest concentrations, respectively. It was therefore assumed that the α will have nucleated and not the γ during these experiments.

3.2 Determination of path length of improved URS:

Prior to each use of the improved URS, the path length needs to be calculated for the temperature range it will be used for. Figure 4Figure 4 shows the change in path length and time of flight over the experimental temperature range from the water calibration.
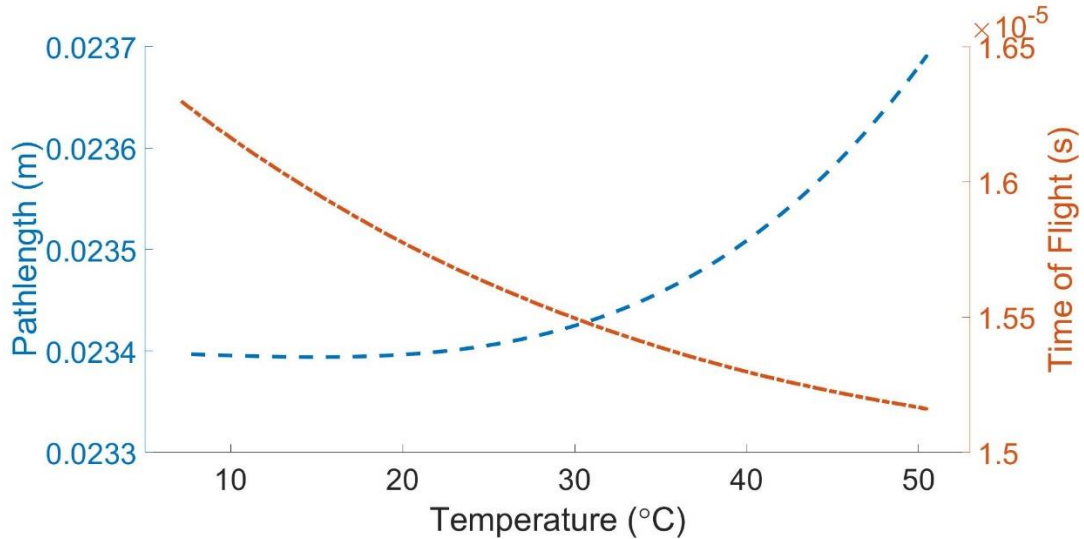
Figure 4 Temperature dependent path length (dashed line) calibration of the improved URS probe obtained using de-ionised water as calibrant together with the speed of sound in pure water from literature, and the corresponding time of flight in the water column (dot dashed line). Path length is determined with an accuracy of +/- 5 x10^{-6} m and a precision of +/- 5 x10^{-7} m from Equation 6 and the fit to the path length is given in Equation 8 where the correlation coefficient R^2 =1

Previous studies (Chávez et al., 1985; Bilaniuk and Wong, 1993) fitted a quintic function to the speed of sound in water; therefore this method was replicated for the calibration.

$$X = -6.2357E^{-14}T^5 + 2.9149E^{-11}T^4 + 2.1039E^{-9}T^3 - 5.5382E^{-8}T^2 - 1.3949E^{-7}T + 0.0234$$

$$(8)$$

Where X is the path length and T is the temperature.

It should be noted that Equation (8)(8) is only accurate for the specific path length used in this study. Here, the path length was not changed between experiments, but a new calibration needs to be performed and a new equation determined when the path length is altered.

3.3 Determination of cloud point and MSZW with optical turbidity corroboration:

Corroboration of the cloud point determination between improved URS and optical turbidity is shown in figure 3.
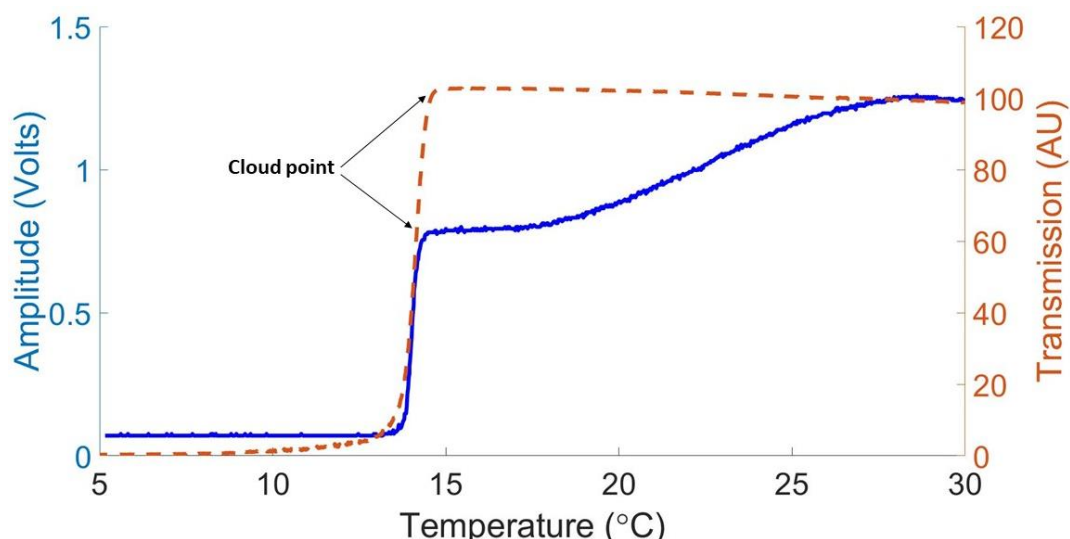
Figure 5 Changes in acoustic amplitude (solid line) and optical transmission (dashed line) throughout cooling crystallisation of a 3.11 mol kg^{-1} aqueous glycine solution, saturated at 30 ^{o}C, cooled at -0.5 ^{o}C min^{-1}.

Figure 3 shows that there are changes which occur in the acoustic amplitude during the cooling of the glycine solution. Interestingly, whilst the optical transmission remains relatively constant at around 100 AU before crystallisation (cloud point), the ultrasound amplitude changes considerably before the crystallisation event occurs.

Between 30 ^{o}C and 14 ^{o}C this is the metastable zone, and no visible crystals were present. A decrease in amplitude between 30 ^{o}C and 14 ^{o}C is suggestive of scattering bodies being produced, so it is possible that a clustering process is occurring in the supersaturated solution. The structure of supersaturated glycine solution is debated (Chattopadhyay et al., 2005; Huang et al., 2008; Friant-Michel and Ruiz-López, 2010; Yani et al., 2012; Zimbitas et al., 2019; Di Gioacchino et al., 2020).

At around 14 ^{o}C there is a sudden decrease in the amplitude of the ultrasound signal and the optical transmission. This is the cloud point, which means nuclei are detectable optically and are causing scattering of the signals. A sudden decrease in acoustic amplitude at 14 ^{o}C is due to nucleation and subsequent crystal growth. At this point, the solution looks turbid due to the presence of crystals that scatter visible light. After this decrease the amplitude plateaus, due to the signal being entirely scattered and consequently not reflected back to the transducer.

Relating this decrease to the nature and quantity of solid material appearing is a challenge which is as yet unresolved, as the complexity of the scattering processes occurring is due to the simultaneous change in size, morphology and amount of crystalline material (Mougin et al., 2002). The point at which the sudden increase in attenuation occurs was determined as the cloud point, or the presence of the first crystal. The attenuation plateaus after further cooling and this is due to a very high number of crystals scattering the sound, with likely multiple scattering effects also occurring.

The MSZW was calculated using equation 1, through measurement of the cloud point and coupled with the solubility data of α-glycine in water (equation 2). Corroboration of the values for the width of the metastable zone between optical turbidity and improved URS are depicted in figure 4.
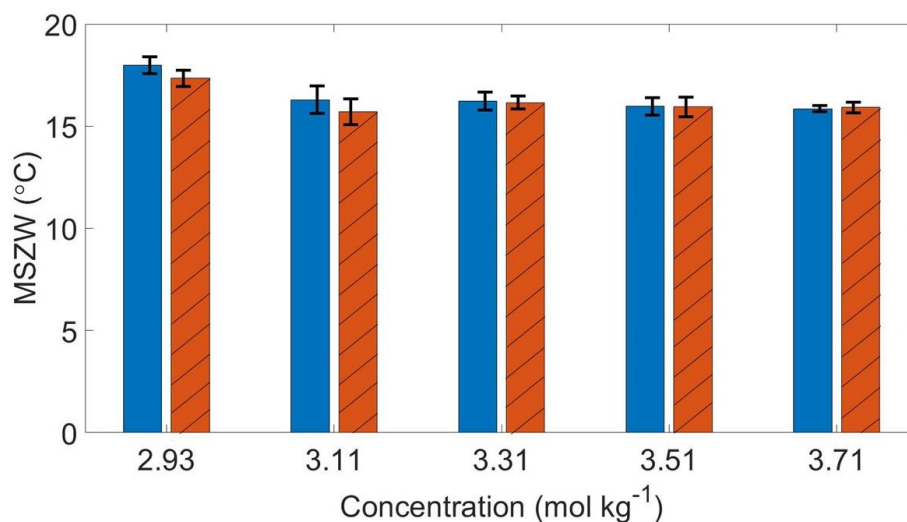

Figure 6 MSZW of α-glycine in water at a cooling rate of -0.5 °C min^{-1} measured by both improved URS (solid bars) and optical turbidity measurements (striped bars). Plotted bars are standard deviation.

Figure 6 shows that there is good agreement between improved URS and optical turbidity in the determination of the MSZW. All measurements agree within the standard deviation. At lower concentrations there is an increase in the MSZW which was recognised by both devices. This is therefore a result of the experimental conditions, rather than the measurement ability.

A Mann Whitney U test was conducted to determine the agreement of the two measurement techniques. The optical cloud point temperature did not differ significantly between the improved URS and optical turbidity measurements, Mann Whitney U test score = 251.000, z-score= -0.297, effect size, r =0.044. Therefore, it is concluded that the two techniques are in good agreement with each other.

For this study, it was decided to determine the MSZW at one cooling rate only, to corroborate the two techniques. Future studies involving multiple cooling rates would be a recommendation for future work.

3.4 Densitometry, velocimetry, and adiabatic compressibility measurements:

Here we demonstrate the ability to calculate the adiabatic compressibility through use of density and ultrasound velocity measurement. Measurements were performed in undersaturated and supersaturated conditions, and not when dispersed crystals were present. It is not suitable to crystallise solutions in the density meter used, and for this reason future work will include in situ density measurement through the improved URS

without the need of a density meter. The density of the glycine solutions with temperature at four different concentrations are shown in Figure 7.
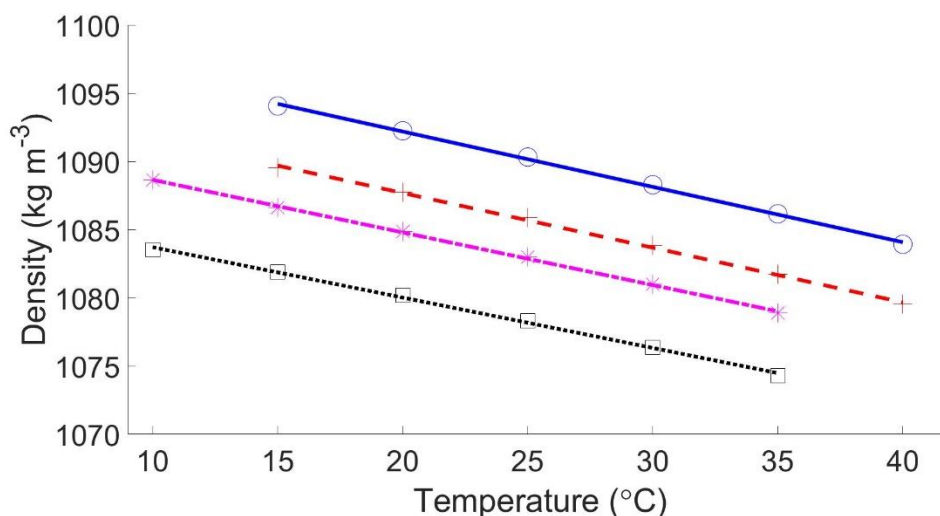

Figure 7 Densities of glycine in water solutions at four different concentrations in both under saturated conditions and within the metastable zone. Solid line - 3.71 mol kg^{-1} aqueous glycine, saturated at 36 °C; dashed line - 3.51 mol kg^{-1} aqueous glycine, saturated at 33 °C; dot-dashed line - 3.31 mol kg^{-1} aqueous glycine, saturated at 30 °C; dotted line - 3.11 mol kg^{-1} aqueous glycine, saturated at 27 °C.

The density of glycine in water solutions was found to increase proportionally to the concentration, which was expected due to the increase in volume fraction of solute, which possesses a density higher than the density of the water. Figure 7 shows that the density increases inversely to the temperature. This is due to the solution occupying a smaller volume as the density increases and hence the volume fraction of glycine increases as the solution volume decreases. The standard deviations of the solutions measured in Figure 7 are all with the resolution of the instrument (±5.00 x10^{-3} kg m^{-3}).

Linear functions were fitted to the averages of density measurements ($r^2 > 0.995$ in all cases). Following the density measurements, velocity measurements were performed for the glycine solution using the improved URS. The results of these measurements across the same temperature range are presented in Figure 8.
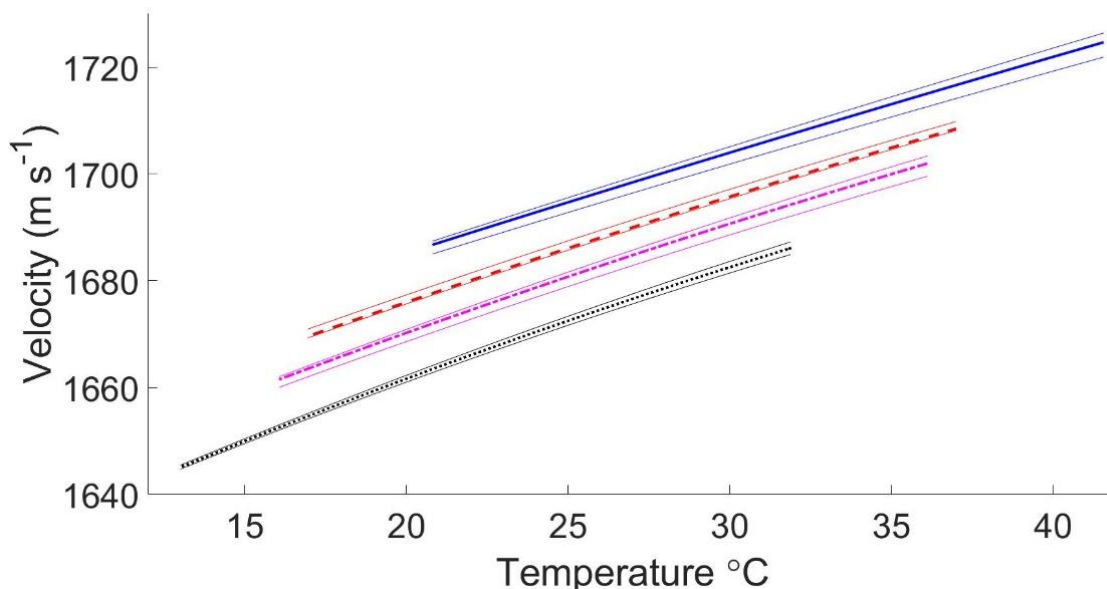
Figure 8 Ultrasound velocity of glycine in water solutions at four different concentrations in both under saturated conditions and within the metastable zone. 95% confidence intervals are plotted for each concentration. Solid line - 3.71 mol kg^{-1} aqueous glycine, saturated at 36 °C; dashed line - 3.51 mol kg^{-1} aqueous glycine, saturated at 33 °C; dot-dashed line - 3.31 mol kg^{-1} aqueous glycine, saturated at 30 °C; dotted line - 3.11 mol kg^{-1} aqueous glycine, saturated at 27 °C.

Figure 8 illustrates the change in ultrasound velocity with temperature. The experiments began at the higher temperature and were cooled at -0.5 °C min^{-1}. All four concentrations used show the same trend, that the ultrasound velocity decreases with the temperature. Speed of sound has been shown to decrease by 3 m s^{-1} °C^{-1} in water (Povey, 1997) so this trend is unsurprising.

The data from Figures 7 (density) and 8 (ultrasonic velocity) were used to calculate adiabatic compressibility using the Wood equation (Equation 7). The adiabatic compressibility of the samples is shown in figure 9.
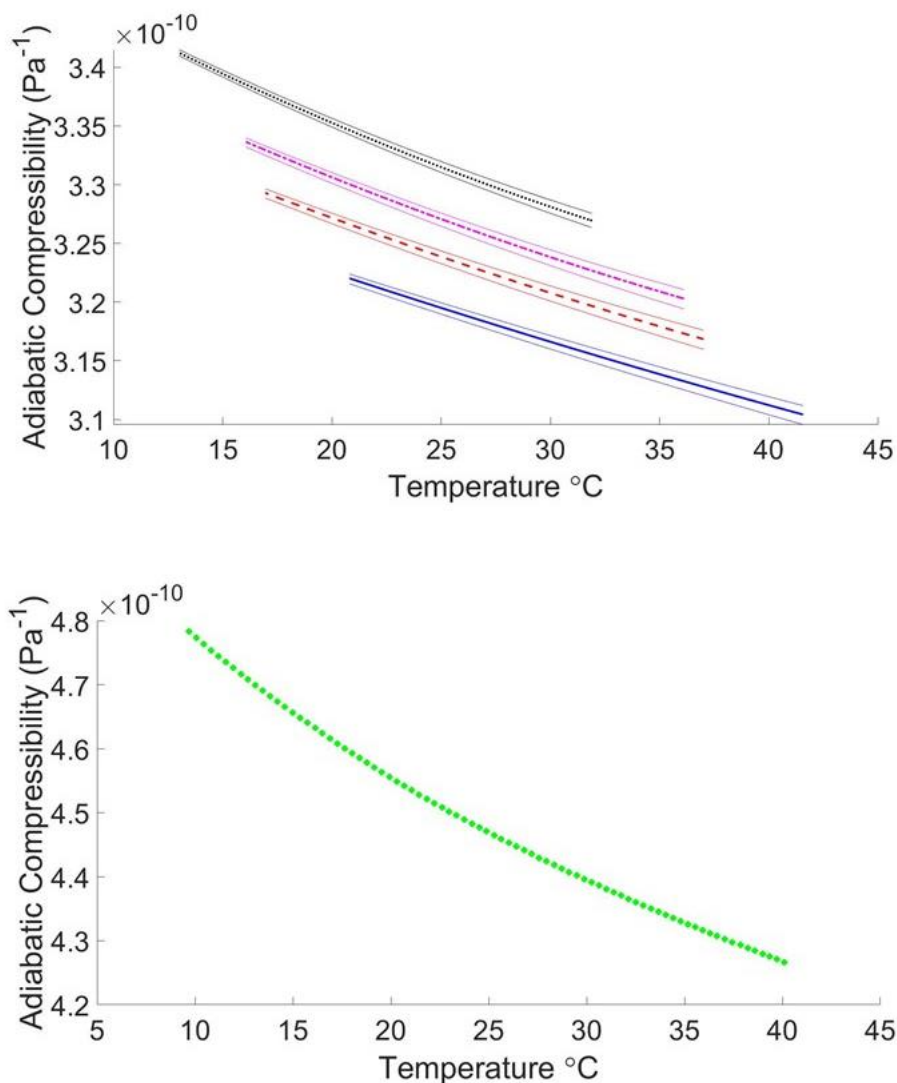
Figure 9 Adiabatic compressibility of water and glycine in water solutions at four different concentrations in both under saturated conditions and within the metastable zone. 95% confidence intervals are plotted for each concentration. Solid line - 3.71 mol kg^{-1} aqueous glycine, saturated at 36 °C; dashed line - 3.51 mol kg^{-1} aqueous glycine, saturated at 33 °C; dot-dashed line - 3.31 mol kg^{-1} aqueous glycine, saturated at 30 °C; dotted line - 3.11 mol kg^{-1} aqueous glycine, saturated at 27 °C; 45° rotated square – water.

Figure 9 shows that the adiabatic compressibility of glycine decreases with an increase in concentration. Furthermore, it is observed that the adiabatic compressibility of all the glycine solutions increased as the solution is cooled. An explanation for the increase in adiabatic compressibility would be that the sample properties are dominated by water which occupies the greater part of the sample volume. It is well accepted that water has unusual material properties, and an increase in adiabatic compressibility below 40 °C due to an expansion of icosahedral water clusters is documented (Fine and Millero, 1973; Loboda and Goncharuk, 2010).

3.5 Power spectrum analysis:

Whilst peak to peak amplitude measurements are useful in the detection of transition temperatures, it does have limitations. There are changes which can occur within a sound pulse, which the amplitude measurement would not detect. To gain more information into crystallisation processes, a frequency domain analysis was performed on the glycine solutions during crystallisation. The power spectrum analysis of a glycine solution is shown in Figure 8.
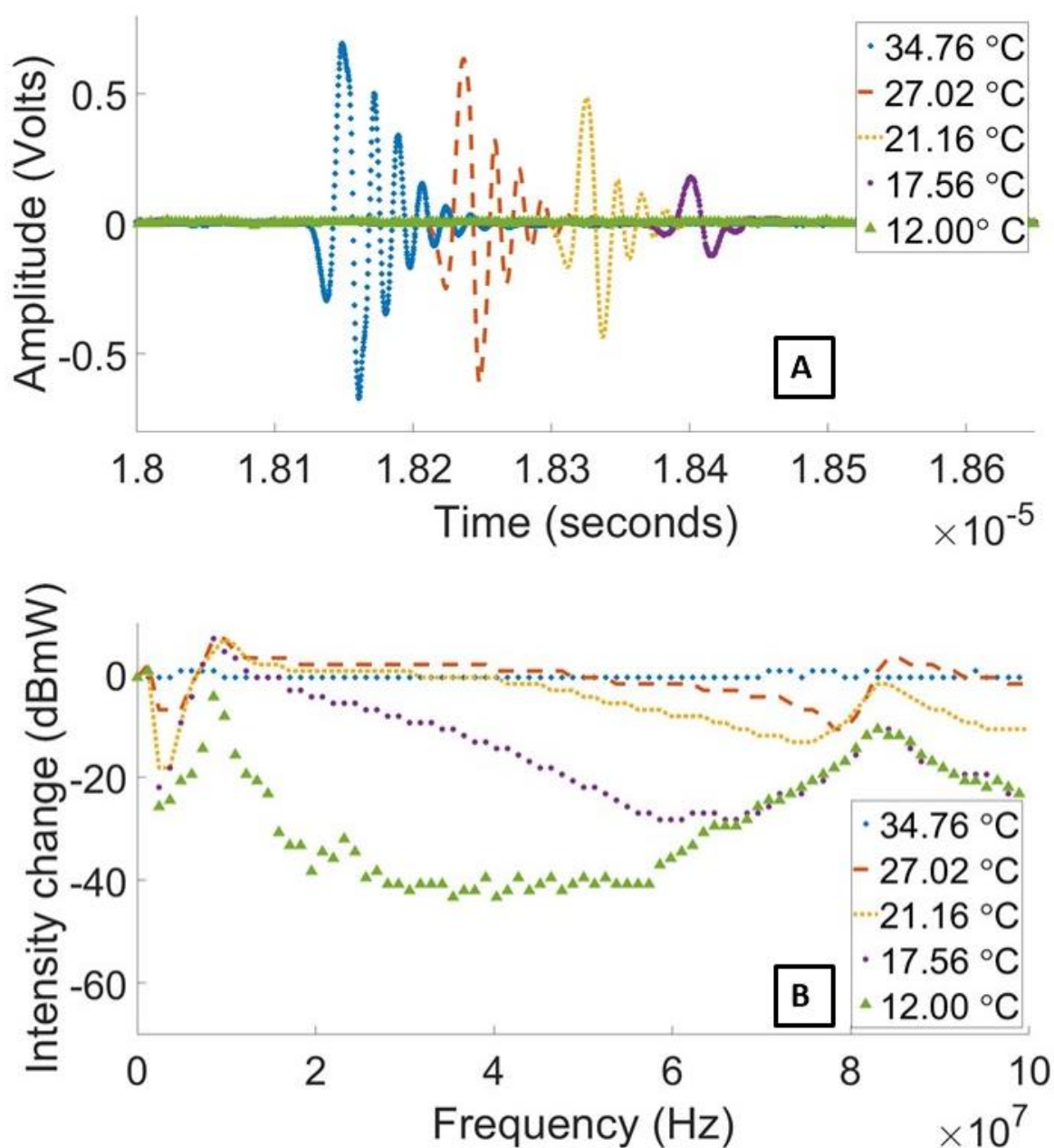

Figure 10 Power spectrum analysis of a 3.11 mol kg^{-1} glycine solution through cooling crystallisation. A consists of five time domain signals, B consists of A's

relative power spectrum. 'O' - data at 34.76 ºC, '+' - data at 27.02 ºC, '*' - data at 21.16 ºC, '□' - data at 17.56 ºC and Δ - data at 12.00 ºC.

FFT analysis of the time resolved signal from URS allows a closer inspection of changes occurring within the sound pulse. Changes occur in the frequency spectra before changes in the peak to peak amplitude occur. The use of frequency space for acoustic analysis is less common than time domain analysis (Reiner et al., 2018).

It can be seen in figures 8A, 8B and 9 that there are changes occurring with regards to the frequency of the sample pulse which would remain undetected by the amplitude measurement alone. The amplitude measurement in this study was peak to peak amplitude. In a sample pulse, the highest crest and lowest trough only are measured in this method of analysis, and hence any change in the smaller peaks within the pulse remain undetected. This is not deemed too much of an issue, as there remains a close agreement between the improved URS and optical transmission; however, figure 8 highlights that there are changes occurring in the sample pulse before the amplitude measure responds. The optical turbidity probe utilised the near IR region with a wavelength of around 700nm. Crystals would not scatter light until they reach this size.

Figures 8A and 8B show that as the temperature decreases, lower frequencies are more attenuated. This is evidenced by their decrease in intensity. In figure 8A the lower frequencies appear earlier in time (on the left side of their respective waveform) whilst the higher frequencies are later in time (on the right side of the waveform). This is evidenced by the decrease in intensity which can be observed in figure 8B and figure 9. Therefore, the lower frequencies are dominating the peak to peak amplitude measurements due to their higher intensity. In figure 9 the fall in intensity of 10 MHz occurs closely to the decrease in optical transmission. Whereas 20 MHz, 30 MHz, 40 MHz and 50 MHz experienced a decrease in intensity before the decrease in optical transmission. It can be seen in figure 8A that the sample pulse changes in terms of the number of wave cycles, with the higher temperature pulses having more cycles than the lower temperature ones. The higher frequencies in the pulse appear later in time than the lower frequencies, this means that the speed of sound is a function of frequency and a detailed analysis of the relationship between the frequency dependent attenuation and velocity might need further analysis, which is beyond the scope of this work.
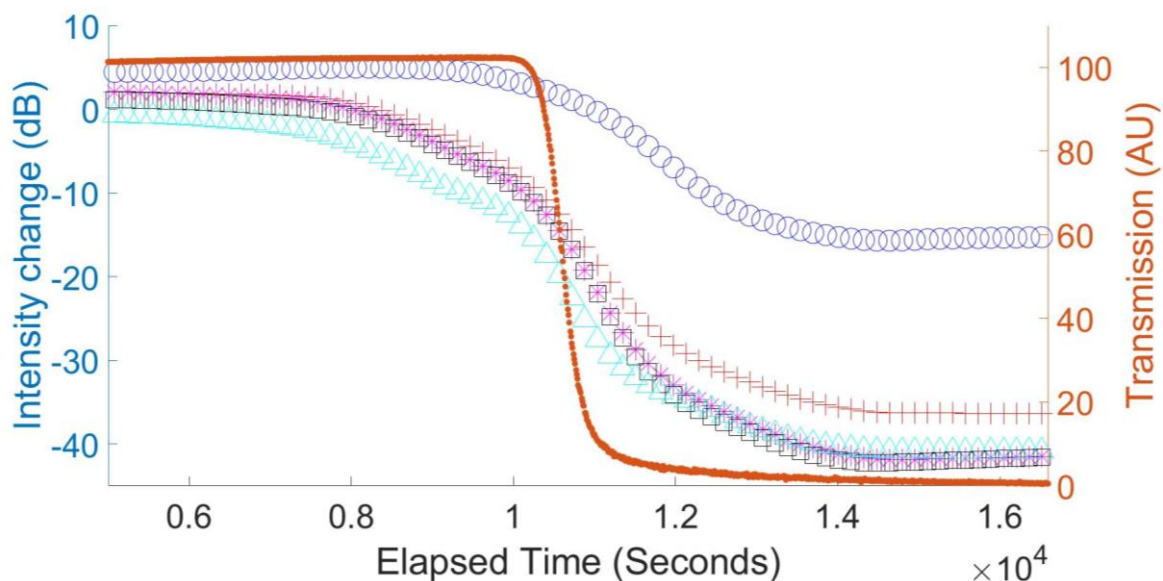
Figure 11 Intensity changes in frequency within the sample pulse from improved URS, derived from figure 8B. Data smoothing used on improved URS data using robust quadratic regression. Optical transmission, '.' is also shown for corroboration. 'O' - 10 MHz, '+' - 20 MHz, '*' - 30 MHz, '□' - 40 MHz, Δ - 50 MHz.

It can be seen in figure 9 that over time each constituent frequency of the sample pulse has a different response in terms of intensity change. Changes at specific frequencies are due to the changing physical properties of the sample medium such as crystal growth, and the crystals become larger as the temperature further decreases and is suggestive of ultrasound scattering bodies prior to the optical transmission response. This question will be addressed in a subsequent paper.

4 Conclusions:

There is strong motivation in industry for effective PAT, here we present a case that this technique can meet this requirement. The improved URS presented here is a powerful tool to study cooling crystallisation of aqueous systems. It can measure ultrasound velocity and attenuation accurately allowing then study of cooling crystallisation in solutions. The MSZW of glycine was determined using attenuation measurements and found to be around 16 $^{\circ}$C at a cooling rate of -0.5 $^{\circ}$C min^{-1}. Using FFT and power spectra measurements, more information can be extracted which will be the subject of a subsequent paper.

The structure of glycine molecules in supersaturated solution remains a debated topic. In this study there is no case presented for a specific self-assembly, but we evidence that changes are occurring within the metastable zone of the supersaturated solution before nucleation and crystallisation occur. Densitometry measurements in tandem with improved URS can quantify the adiabatic compressibility of a sample, however there is a need for in situ density measurement.

The determination of cloud point by URS measurements are in close agreement with those of optical turbidity and hence the MSZW determined by URS is on the same

order of accuracy optical turbidity measurement. Improved URS appears to respond to phase changes earlier than optical turbidity measurement and standard time domain acoustic measurements. The results presented here confirm that acoustic measurements are appropriate as crystallisation PAT.

It would be useful for the use of this technique to be expanded beyond crystalline phase transitions. The opportunity to utilise this technique is vast and future work should be considered.

5 References:

Akulichev, V.A. and Bulanov, V.A. 1983. Crystallization Nuclei in Liquid in a Sound Field. *International Journal of Heat and Mass Transfer*. **26**(2), pp.289–300. DOI:10.1016/S0017-9310(83)80033-7

Barrett, P. and Glennon, B. 2002. Characterizing the metastable zone width and solubility curve using lasentec FBRM and PVM. *Chemical Engineering Research and Design*. **80**(7), pp.799–805. DOI:10.1205/026387602320776876

Bilaniuk, N. and Wong, G.S.K. 1993. Speed of sound in pure water as a function of temperature. *Journal of the Acoustical Society of America*. **93**(3), pp.1609–1612. DOI:10.1121/1.406819

Borji, A. and Jourani, A. 2018. Spectrophotometry as a Method for the Determination of Solubility of Sucrose in Water and Metastable Zone Width of its Aqueous Solutions. *Crystal Research and Technology*. **53**(6), pp.1–6. DOI:10.1002/crat.201700123

Burbidge, A.S., Bridgewater, J. and Saracevic, Z. 1995. Liquid Migration in Paste Extrusion. *Institution of Chemical Engineers*. **73**(Part A), pp.810–816. DOI:10.1016/S0076-6879(08)03802-0

Callahan, C.J. and Ni, X.W. 2012. Probing into nucleation mechanisms of cooling crystallization of sodium chlorate in a stirred tank crystallizer and an oscillatory baffled crystallizer. *Crystal Growth and Design*. **12**(5), pp.2525–2532. DOI:10.1021/cg300135w

Chattopadhyay, S., Erdemir, D., B Evans, J.M., Ilavsky, J., Amenitsch, H., Segre, C.U. and Myerson, A.S. 2005. SAXS Study of the Nucleation of Glycine Crystals from a Supersaturated Solution. *Crystal Growth & Design*. **5**(2), pp.523–527. DOI:10.1021/cg0497344

Chávez, M., Sosa, V. and Tsumura, R. 1985. Speed of sound in saturated pure water. *Journal of the Acoustical Society of America*. **77**(2), pp.420–423. DOI:10.1121/1.391861

Correia, P., Lopes, C., Piedade, M.E.M., Lourenço, J.A.A. and Serrano, M.L. 2006. Solubility and metastable zone width of 1-keto-1,2,3,4-tetrahydro-6-methylcarbazole in acetone. *Journal of Chemical and Engineering Data*. **51**(4), pp.1306–1309. DOI:10.1021/je0600552

Dickinson, E., Kruizenga, F.J., Povey, M.J.W. and van der Molen, M. 1993. Crystallization in oil-in-water emulsions containing liquid and solid droplets. *Colloids and Surfaces A: Physicochemical and Engineering Aspects*. **81**(C), pp.273–279. DOI:10.1016/0927-7757(93)80255-D

Fine, R.A. and Millero, F.J. 1973. Compressibility of water as a function of temperature and pressure. *The Journal of Chemical Physics*. **59**(10), pp.5529–5536. DOI:10.1063/1.1679903

Francis, M.J., Glover, Z.J., Yu, Q., Povey, M.J. and Holmes, M.J. 2019. Acoustic characterisation of pH dependant reversible micellar casein aggregation. *Colloids and Surfaces A: Physicochemical and Engineering Aspects*. **568**(February), pp.259–265. DOI:10.1016/j.colsurfa.2019.02.026

Friant-Michel, P. and Ruiz-López, M.F. 2010. Glycine Dimers: Structure, Stability, and Medium Effects. *ChemPhysChem*. **11**(16), pp.3499–3504. DOI:10.1002/cphc.201000354

Fujiwara, M., Chow, P.S., Ma, D.L. and Braatz, R.D. 2002. Paracetamol Crystallization Using Laser Backscattering and ATR-FTIR Spectroscopy: Metastability, Agglomeration, and Control. *Crystal Growth and Design*. **2**(5), pp.363–370. DOI:10.1021/cg0200098

García-Álvarez, J., García-Hernández, M.J., Novoa-Díaz, D.F., Turó Peroy, A., Chávez Domínguez, J.A. and Salazar Soler, J. 2013. Resizing buffer rods for ultrasound testing of food products with acoustic noise considerations. *Ultrasonics*. **53**(1), pp.294–301. DOI:10.1016/j.ultras.2012.06.013

Di Gioacchino, M., M, A.R., Imberti, S., Holzmann, N., Bruni, F., Ricci, M.A., Imberti, S., Holzmann, N. and Bruni, F. 2020. Hydration and aggregation of a simple amino acid: The case of glycine. *Journal of Molecular Liquids*. **301**, p.112407. DOI:10.1016/j.molliq.2019.112407

Hennessy, A., Neville, A. and Roberts, K.J. 2004. In-situ SAXS/WAXS and turbidity studies of the structure and composition of multihomologous n-alkane waxes crystallized in the absence and presence of flow improving additive species *In*: *Crystal Growth and Design*., pp.1069–1078. DOI:10.1021/cg0341050

Hindle, S.A., Povey, M.J.W. and Smith, K.W. 2002. Characterising Cocoa Butter Seed Crystals by the Oil-in-Water Emulsion Crystallization Method. *Journal of the American Oil Chemists' Society*. **79**(10), pp.993–1002.

Huang, J., Stringfellow, T.C. and Yu, L. 2008. Glycine Exists Mainly as Monomers, Not Dimers, in Supersaturated Aqueous Solutions: Implications for Understanding Its Crystallization and Polymorphism. *Journal of the American Chemical Society*. **130**, pp.13973–13980. DOI:10.1021/ja804836d

Kulmyrzaev, A., Cancelliere, C. and McClements, D.J. 2000. Characterization of aerated foods using ultrasonic reflectance spectroscopy. *Journal of Food Engineering*. **46**(4), pp.235–241. DOI:10.1016/S0260-8774(00)00070-4

Liang, K., White, G., Wilkinson, D., Ford, L.J., Roberts, K.J. and Wood, W.M.L. 2004. Examination of the Process Scale Dependence of L-Glutamic Acid Batch Crystallized from Supersaturated Aqueous Solutions in Relation to Reactor Hydrodynamics. *Industrial & Engineering Chemistry Research*. **43**, pp.1227–1234. DOI:10.1021/ie0305014

Loboda, O. and Goncharuk, V. 2010. Theoretical study on icosahedral water clusters. *Chemical Physics Letters*. **484**, pp.144–147.

Lyczko, N., Espitalier, F., Louisnard, O. and Schwartzentruber, J. 2002. Effect of ultrasound on the induction time and the metastable zone widths of potassium sulphate. *Chemical Engineering Journal*. **86**(3), pp.233–241. DOI:10.1016/S1385-8947(01)00164-4

Marciniak, B. 2002. Density and ultrasonic velocity of undersaturated and supersaturated solutions of fluoranthene in trichloroethylene, and study of their metastable zone width. *Journal of Crystal Growth*. DOI:10.1016/S0022-0248(01)02088-7

Mougin, P., Wilkinson, D., Roberts, K.J. and Tweedie, R. 2002. Characterization of particle size and its distribution during the crystallization of organic fine chemical products as measured in situ using ultrasonic attenuation spectroscopy. *The Journal of the Acoustical Society of America*. **109**(1), pp.274–282. DOI:10.1121/1.1331113

Nalesso, S., Bussemaker, M.J., Sear, R.P., Hodnett, M. and Lee, J. 2019. A review on possible mechanisms of sonocrystallisation in solution. *Ultrasonics Sonochemistry*. DOI:10.1016/j.ultsonch.2019.04.020

Parsons, A.R., Black, S.N. and Colling, R. 2003. Automated measurement of metastable zones for pharmaceutical compounds. *Chemical Engineering Research and Design*. **81**(6), pp.700–704. DOI:10.1205/026387603322150552

Povey, M.J.W. 2016. Nucleation in food colloids. *The Journal of Chemical Physics*. **145**(21), p.211906. DOI:10.1063/1.4959189

Povey, M.J.W. 1997. *Ultrasonic Techniques for Fluids Characterization*. San Diego, Calif. ; London: Academic Press. DOI:10.1016/b978-0-12-563730-5.x5000-4

Povey, M.J.W. 2013. Ultrasound particle sizing: A review. *Particuology*. **11**(2), pp.135–147. DOI:10.1016/j.partic.2012.05.010

Povey, M.J.W., Hindle, S.A., Aarflot, A. and Hoiland, H. 2006. Melting Point Depression of the Surface Layer in n-Alkane Emulsions and Its Implications for Fat Destabilization in Ice Cream. *Crystal Growth & Design*. **6**(1), pp.297–301. DOI:10.1021/cg030051i

Rahman, M.A. and Rahman, M.M. 2015. Determination of the Metastable Zone Width, Nucleation Kinetics, Structural and Optical Properties of KCl Doped KAP Crystal. *Journal of Crystallization Process and Technology*. **05**(02), pp.31–42. DOI:10.4236/jcpt.2015.52005

Sangwal, K., Mielniczek-Brzóska, E. and Barylska, S. 2014. Solubility of ammonium oxalate in water-acetone mixtures and metastable zone width of their solutions. *Chemical Engineering Research and Design*. **92**(3), pp.491–499. DOI:10.1016/j.cherd.2013.08.031

Sharma, S.K., Thakur, A., Kumar, D. and Nathan, V. 2020. Thermophysical properties of glycine and glycylglycine in aqueous tartaric acid at different temperatures: Volumetric, acoustic and viscometric studies. *Journal of Molecular Liquids*. **297**, p.111941. DOI:10.1016/j.molliq.2019.111941

Simon, L.L., Pataki, H., Marosi, G., Meemken, F., Hungerbühler, K., Baiker, A., Tummala, S., Glennon, B., Kuentz, M., Steele, G., Kramer, H.J.M., Rydzak, J.W., Chen, Z., Morris, J., Kjell, F., Singh, R., Gani, R., Gernaey, K. V, Louhi-Kultanen, M., O'Reilly, J., Sandler, N., Antikainen, O., Yliruusi, J., Frohberg, P., Ulrich, J., Braatz, R.D., Leyssens, T., von Stosch, M., Oliveira, R., Tan, R.B.H., Wu, H., Khan, M., O'Grady, D., Pandey, A., Westra, R., Delle-Case, E., Pape, D., Angelosante, D., Maret, Y., Steiger, O., Lenner, M., Abbou-Oucherif, K., Nagy, Z.K., Litster, J.D., Kamaraju, V.K. and Chiu, M.-S. 2015. Assessment of Recent Process Analytical Technology (PAT) Trends: A Multiauthor Review. *Organic Process Research & Development*. **19**(1), pp.3–62. DOI:10.1021/op500261y

Spieweck, F. and Bettin, H. 1992. Review: Solid and liquid density determination. *Technisches Messen*. **59**(7–8), pp.285–292. DOI:10.1524/teme.1992.59.78.285

Tong, J. and Povey, M.J.W. 2002. Pulse echo comparison method with FSUPER to measure velocity dispersion in n-tetradecane in water emulsions. *Ultrasonics*. **40**, pp.37–41.

Ulrich, J. and Strege, C. 2002. Some aspects of the importance of metastable zone width and nucleation in industrial crystallizers. *Journal of Crystal Growth*. DOI:10.1016/S0022-0248(01)02284-9

Yang, X., Wang, X. and Ching, C.B. 2008. Solubility of Form α and Form γ of Glycine in Aqueous Solutions. *Journal of Chemical & Engineering Data*. **53**(5), pp.1133–1137. DOI:10.1021/je7006988

Yani, Y., Chow, P.S. and Tan, R.B.H. 2012. Glycine Open Dimers in Solution: New Insights into α-Glycine Nucleation and Growth. *Crystal Growth & Design*. **12**(10), pp.4771–4778. DOI:10.1021/cg300452n

Zimbitas, G., Jawor-Baczynska, A., Vesga, M.J., Javid, N., Moore, B.. B.D., Parkinson, J. and Sefcik, J. 2019. Investigation of molecular and mesoscale clusters in undersaturated glycine aqueous solutions. *Colloids and Surfaces A: Physicochemical and Engineering Aspects*. **579**(July), p.123633. DOI:10.1016/j.colsurfa.2019.123633

6 Conflict of interest statement:

The authors declare that they have no known competing financial interests or personal relationships that could have appeared to influence the work reported in this paper.

7. Funding Sources: